Optica Applicata, Vol. XXXV, No. 3, 2005

Infrared second-order nonlinear optical effect in Sb_2Te_3–$SrBr_2$–$PbCl_2$ glass

WOJCIECH GRUHN

Institute of Physics, Jan Długosz University, al. Armii Krajowej 13/15, 42-200 Częstochowa, Poland

A phenomenological and microscopic theory of IR picosecond nonlinear optical response in glass is developed for the middle IR spectral range (5–15 μm). Both IR-induced second harmonic generation (SHG) as well as linear electrooptic effect (LEOE) were observed. The observed effects are explained within a framework of fifth-order nonlinear optical susceptibilities. A model that reproduces the basic features of the experimental data, in which are discovered the optical nonlinearities caused by photoinduced electron–phonon anharmonic interactions, is proposed. The role of the IR induced phase matching conditions in the observed phenomena is discussed.

Keywords: photoinduced second harmonic generation, Sb_2Te_3–$SrBr_2$–$PbCl_2$ glass.

1. Introduction

It is well known that the second-order nonlinear optical effects such as second harmonic generation (SHG) and linear electrooptic effect (LEOE) are forbidden by symmetry [1] in glasses. An external electric field is usually applied to induce non-centrosymmetry (electric field induced second-order optical effects) [2]. Unfortunately this method cannot be applied for the infrared materials, which are transparent in the middle-IR spectral region, due to the appearance of electroconductivity. However, the possibility to operate the optical constants of glasses in the middle-IR spectral range is very important when using the optical fibers for the CO- and CO_2-lasers [3–5].

For the reasons presented above, the IR optical poling [6, 7] in glasses becomes increasingly attractive, since it offers optically operated waveguides for recording and transmission of IR-information. Up to date, all the investigations in the femtosecond regime were performed for the near-IR less than 3 μm wavelengths [8, 9]. Among the IR materials, chalcohalide and chalcogenide glasses [10–13] are most promising. The photoinduced changes in the chalcogenide glasses have been well studied for visible and near-IR spectral range [13]. However, physical origin of the photoinduced changes of second-order nonlinear optical properties is principally different for the middle-IR spectral range. The principal difference consists in commensurability of the middle-IR frequencies with the phonon frequencies of the glasses [8]. As a consequence one can expect a substantial contribution of the optically induced

electron–phonon interactions (EPI) to the second-order optical susceptibilities [12]. The EPI are described by third order derivatives of the electrostatic potential [14] due to relatively high CO-laser photoexcited power density. In this case, the second-order nonlinear optical effects might be enhanced. However, following general phenomenological considerations [1, 2] one can expect a necessity to introduce the nonlinear optical susceptibilities of higher orders.

In this paper, there is proposed a new type of IR optical poling consisting in photo-pumping of appropriate phonon and electronic states using the IR pulsed CO-laser ($\lambda = 5.5$ μm). It is explored how a time-resolved, nonlinear optical spectroscopy of the glasses may be applied to investigate EPI and dynamics of the external IR pump light in the glasses. The novel nonlinear optical effect related to the IR photoinduced anharmonic lattice-electron interaction is presented. As a consequence, the optically induced electron–phonon anharmonic non-centrosymmetry appears in the electronic charge density distribution of a particular glass structural cluster. In the traditional all-optical technique [15], this method is explained by means of three main physical principles: a net orientation of particular clusters, a photoexcited resonance-selective excitation and an electric field induced SHG. In the case of the IR optical poling the photoinduced non-centrosymmetry of the photoexcited phonons begins to play crucial role and it is necessary to consider a process of interactions of at least two photons and three phonons or a fifths-order process. The interactions with one phonon could not contribute to the harmonic electron–phonon interactions, so we will consider only anharmonic electron–phonon interactions with at least three phonons.

2. Theoretical approach

Because the non-centrosymmetric photoinduced electron–phonon anharmonicity requires participation of at least three phonons, otherwise we would have a harmonic electron–phonon interactions which would not lead to the non-centrosymmetry, the SHG effect should be described by an equation:

$$P_i = \chi_{ijklmn} E_j^{(\omega)} E_k^{(\omega)} E_l^{(\Omega_1)} E_m^{(\Omega_2)} E_n^{(\Omega_3)} \tag{1}$$

where P_i is the optical polarization of the medium, χ_{ijklmn} is the six-order tensor describing the fifth-order nonlinear optical (NLO) susceptibility, $E_l^{(\Omega_1)}$, $E_m^{(\Omega_2)}$, $E_n^{(\Omega_3)}$ are the interacting phonon's displacive vectors (induced by pump light) participating in the photoinduced anharmonic EPI process; $E_j^{(\omega)}$, $E_k^{(\omega)}$ are the electric strength of electromagnetic beams with polarization k and j, respectively. The considered process is substantially a multi-photon process [15]. We have done the microscopic calculations using the Green function method [16] for numerical evaluations of IR-induced charge density non-centrosymmetry caused by anharmonic EPI. The electronic structure calculations were done using the norm conserving non-local pseudopotential method [17, 18] to evaluate values of the photoinduced EPI. Due to the reasons presented

above, space derivatives of the appropriate electrostatic potentials (determining the anharmonic electron-photon interactions) were calculated. The latter are necessary for calculations of harmonic and anharmonic phonon contributions to the appropriate nonlinear optical susceptibilities. More detailed calculation technique is given in [19].

In the case of the LEOE effect the phenomenology is similar to the former case:

$$P^{(2\omega)}(\mathbf{r}, t) = \varepsilon_0 \Big\{ \langle \left| E_{\mathrm{pr}}^{(\omega)}(\mathbf{r}, t-\tau) \right| \left[E^{\Omega_1 + \Omega_2 + \Omega_3}(\mathbf{r}, t) \right]^2 \rangle + \langle \left| E_{\mathrm{pump}}^{(\omega)}(\mathbf{r}, t) \right| \left[E^{\Omega_1 + \Omega_2 + \Omega_3}(\mathbf{r}, t) \right]^2 \rangle \Big\} \tag{2}$$

where $E_{\mathrm{pr}}^{(\omega)}(\mathbf{r}, t-\tau)$ is the electric strength of probing beam, $E^{\Omega_1 + \Omega_2 + \Omega_3}(\mathbf{r}, t)$ is the electric strength caused by phonons with frequencies Ω_1, Ω_2, Ω_3, $E_{\mathrm{pump}}^{(\omega)}(\mathbf{r}, t)$ is the electric strength of pumping beam, and τ is a pump-probe delaying time shift. The system of appropriate differential equations with varied delaying time between the pumping and probing laser beams was proposed. We took also into account the photo-occupation energy level dynamics due to the IR photoinduced changes. This approach automatically included interactions between the fundamental and the doubled frequency of the IR beams [8, 9].

Our calculations have shown that the Sb–Te clusters in the Sb_2Te_3–$SrBr_2$–$PbCl_2$ glass played dominant role in the corresponding photoinduced optical susceptibilities. For the Ba–Br and Pb–Cl clusters the IR-induced changes were relatively low (less than 1.6%). For example, the matrix dipole moments in the case of Sb–Te bonds were equal to about 0.882 debye (D). For comparison, the total dipole moments are equal to 0.018 and 0.091 D, for the Ba–Br and Pb–Cl bonds, respectively. The process of interaction of the probing $E_{\mathrm{pr}}^{(\omega)}(\mathbf{r}, t)$ CO_2-laser beam with the investigated medium may be also described as follow:

$$E(\mathbf{r}, t) = E_{\mathrm{pr}}^{(\omega)}(\mathbf{r}, t) + E_{\mathrm{pr}}^{(\omega)}(\mathbf{r}, t) + E_{\mathrm{pump}}^{(\omega_p)}(\mathbf{r}, t) + E^{(\Omega_1 + \Omega_2 + \Omega_3)}(\mathbf{r}, t-\tau) \tag{3}$$

where Ω_1, Ω_2 and Ω_3 and are the frequencies of phonons effectively participating in the appropriate anharmonic electron–phonon interactions. The interacting photons are expressed in the plane wave presentation:

$$E_{\mathrm{pr}}^{(\omega)}(\mathbf{r}, t) = E^{(0)} \exp\left[i(\omega t + \mathbf{k} \cdot \mathbf{r} + \phi_1) \right] \tag{4}$$

where $E^{(0)}$ and ϕ_1 are the amplitude and phase of the electromagnetic probe wave with a frequency ω at the moment in time t at the point of space $\mathbf{r}$, respectively, and $\mathbf{k} \cdot \mathbf{r}$ is a scalar product.

The appearance of a term with the frequency 2ω is caused by photoinduced non-centrosymmetry and is similar to the process of interference between two coherent

waves with fundamental and doubled frequencies [20]. The temporally averaged output nonlinear polarization for the doubled frequency was expressed in a form:

$$P^{(2\omega)}(\mathbf{r}, t) \cong \varepsilon_0 \left| E_{\mathrm{pr}}^{(\omega)}(\mathbf{r}, t-\tau) \right|^2 \Big\{ \langle E_{\mathrm{pump}}^{\omega_p}(\mathbf{r}, t) \left[E^{\Omega_1 \pm \Omega_2 \pm \Omega_3}(\mathbf{r}, t) \right]^2 \rangle + \langle E_{\mathrm{pr}}^{\omega}(\mathbf{r}, t) \left[E^{\Omega_1 \pm \Omega_2 \pm \Omega_3}(\mathbf{r}, t) \right]^2 \rangle + \langle E_{\mathrm{pr}}^{2\omega}(\mathbf{r}, t) \left[E^{\Omega_1 \pm \Omega_2 \pm \Omega_3}(\mathbf{r}, t) \right]^2 \rangle \Big\} \quad (5)$$

where the brackets mean temporal averaging.

The first term corresponds to the interaction between the pump CO-laser beam and the modulated photoexcited non-centrosymmetry anharmonic phonon modes possessing the frequencies $\Omega_1 \pm \Omega_2 \pm \Omega_3$ responsible for anharmonic interactions. The second and third ones are responsible for electron–phonon interaction frequencies ω and 2ω, respectively. These terms are responsible for the appearance of the photoinduced non-centrosymmetry in the given point of the media (**r**). The amplitudes of the photoinduced anharmonic modes ($E^{\Omega_1 \pm \Omega_2 \pm \Omega_3}(\mathbf{r}, t)$) are proportional to the pumping photoinduced IR power density. From the general symmetry considerations of the glass cluster it was concluded that maximal output SHG was observed for parallel polarisation of the pumping and probing beams. This one reflects the fact that the direction of the photoinduced charge density shift should be always parallel to the pumping CO-laser polarization. The effect of second-order optical effect's appearance was observed because there exists a range of phonon frequencies satisfying conditions $\omega - \omega_1 \pm \Omega_1 \pm \Omega_2 \pm \Omega_3 = 0$ which are necessary for an occurrence of the non-centrosymmetry tensor components during the picosecond photoexcitation.

When one takes into account the nonlinear interactions between the fundamental (probe) wave with the vector $\mathbf{k}_{\mathrm{pr}}^{(\varpi)}$, doubled frequency wave with the vector $\mathbf{k}^{(2\omega)}$, pump wave with the vector $\mathbf{k}_{\mathrm{pump}}^{(\varpi_p)}$ as well the photoinduced combined anharmonic frequencies with the wave vectors $\mathbf{K}^{\Omega_1 + \Omega_2 + \Omega_3}$, a wide spectrum of angles satisfying the phase matching conditions is received:

$$P^{(2\omega)}(\mathbf{r}, t) \cong \varepsilon_0 \chi^{(5)}(2\omega; \omega_p, \omega, \Omega_1, \Omega_2, \Omega_3) \left| E_{\mathrm{pr}}^{(2\omega)}(\mathbf{r}, t-\tau) \right|^2 \exp\left(-i \Delta\mathbf{k} \cdot \mathbf{r} \right) \quad (6)$$

where $\Delta\mathbf{k} = \mathbf{k}^{(2\omega)} - \mathbf{k}_{\mathrm{pr}}^{(\omega)} \pm \left(\mathbf{k}_{\mathrm{pump}}^{(\omega)} + \mathbf{K}^{(\Omega_1 + \Omega_2 + \Omega_3)} \right)$ and $\Delta\mathbf{k} \cdot \mathbf{r}$ is a scalar product, $\chi^{(5)}$ is the fifth-order optical susceptibility.

The range of angles satisfying the phase synchronism conditions will be in this case relatively large because there exist large groups of phonons satisfying phase matching conditions within the spectral range 5–8 μm.

3. Experimental

For an experimental verification of the proposed theoretical approach, Sb_2Te_3–$SrBr_2$ –$PbCl_2$ glasses were chosen because these glasses possess higher transparency in

the spectral range 5–10 μm comparing with the known [12] ones. The calculated theoretical dependences of the SHG versus the photoinducing power and temperature are presented in Fig. 1. The performed calculations predicted an increase in the photoinduced SHG with increasing IR-induced intensity and with decreasing temperature. The SHG was determined by the Maker fringes method [21] done for 5 specimens with the same content. The equipment allowed performing the measurements of the optical SHG and LEOE. The pulsed CO-laser (λ = 5.5 μm, P = 12–28 MW, τ = 0.44–80 ps, frequency repetition 8–15 Hz) served as IR pumping light. We used Q-switched CO_2-laser beam (λ = 10.6 μm, P = 25 MW; τ = 2–10 ps) for the SHG as the probing beam. This laser was synchronized in time with the CO-laser beam (λ = 5.5 μm). Thermoregulated system UTREX was used for regulation and stabilization of the temperature. For the LEOE measurements, as a probe beam, we used continues He-Ne laser with the wavelength of 3.39 μm and power of about 65 mW/cm^2. The probe beam diameter was equal to about 8 mm. The pumping CO-laser energy was chosen to avoid sample overheating. An IR bolometer, connected with an electronic boxcar integration (gain time up to 420 ps), was used for detection of the output SHG signal. The laser beam has been moved through the surface to average the sample surface non-homogeneity with the varying incident angle within the range from – 60° to 60°. The Maker fringe pattern possessed a good symmetry and the SHG output signal achieved a maximum at angles lying within the range from 55° to 65°. The intensity of the output SHG was varied within the range from 10^{-6} to 10^{-7} with respect to fundamental beam, which corresponds to susceptibility about several fm/V. The calculations of the SHG tensor values were done taking into account the Fresnel losses, Gaussian-like profile of the beam, optical attenuation, as well as the appearance of the photoinduced birefringence (10^{-1}–10^{-2}). The performed

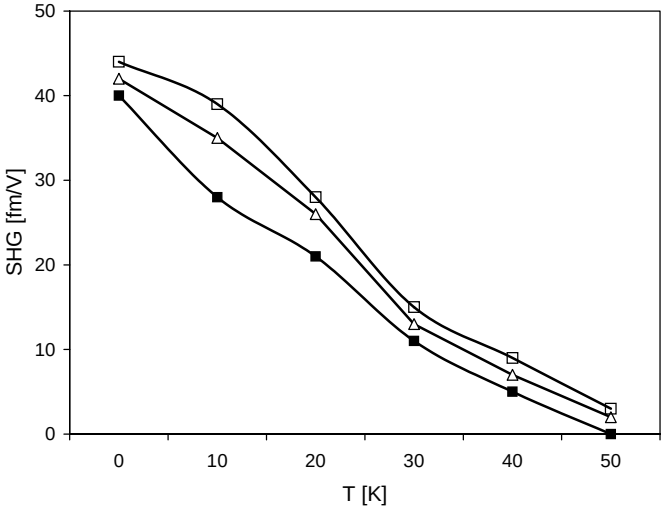

Fig. 1. Temperature dependence of the SHG at different pumping power densities: 0.5 GW/cm^2 (■), 1 GW/cm^2 (△), 1.5 GW/cm^2 (□).

calculations have shown that the maximal output SHG exists for the parallel polarization of inducting and probing laser beams. The angle between these beams did not exceed 4°. The fluorescence signal appeared for the spectral wavelengths below 3.8 μm and was spectrally slightly separated by a grating IR monochromator SP-3M (spectral resolution of 7 nm/mm). The time duration of the SHG signal was equal to about 1.2 ps. The statistics of the output SHG signal satisfied the Student test with an accuracy of better than 0.03. The reflectivity of the samples was equal to 20%. Every SHG value was obtained after averaging by 200–300 pulses.

4. Results and discussion

The measurements of the photoinduced birefringence and evaluations of the corresponding LEOE coefficients (at T = 4.2 K) were done using a Senarmont schema [22]. The magnetooptical lock-in modulation of He-Ne laser polarization allowed to enhance the precision of the birefringence evaluation up to 10^{-7}. As in the case of the SHG, we have found that the maximal electro-optical effect (EOE) signal is achieved for the parallel polarization of the pumping and probing beams. The SHG was measured by the method described in [19].

In Figure 2 the measured dependences of the $\chi^{(5)}$ versus CO-laser pump power (λ = 5.5 μm) are presented. An increase in the SHG versus the pumping CO-laser power within 0 to 1.8 GW/cm^2 was observed. With a decreasing temperature, the values of the photoinduced SHG increase achieving a relatively large value (about 50 fm/V). All the experimental values of SHG converge to about 50 fm/V when the light intensity tends to 1.76 GW/cm^2. The diagonal tensor components $\chi^{(5)}_{ijklm}$ values were larger than all off-diagonal tensor components of about one order of magnitude. For the pumping power higher than 1.78 GW/cm^2 the photochemical destruction has

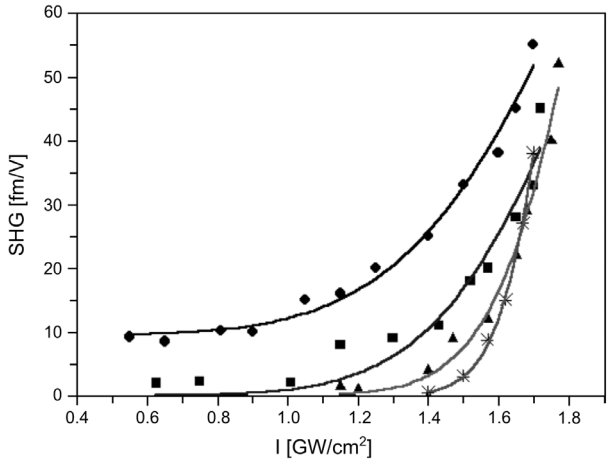

Fig. 2. Photoinduced SHG *vs.* the pumping CO-laser power I at different values of applied temperature T: 4.2 K (●), 13.5 K (■), 25 K (▲), 45 K (✳).

appeared. For comparison, it was also presented in Fig. 1 together with calculated SHG. A good agreement between the theoretical curves and experimental results was observed. The main discrepancies appeared for the temperature of about 13.5 K for the pumping powers within the 1.0–1.3 GW/cm^2 range. It reflected substantial disturbances of the phase matching conditions for these pumping power ranges, probably due to a spatial glass non-homogeneity.

The fluorescence spectra showed a signal in the range of 2–3 μm. Thus it was outside the spectral range for the fundamental and doubled frequency spectral region. The maximal SHG signal was observed for the pump-probing delaying time of about 28 ps.

The fifth-order tensor component in the case of the LEOE was expressed as an interaction of the low-power IR poling beam with a frequency ω with the grating

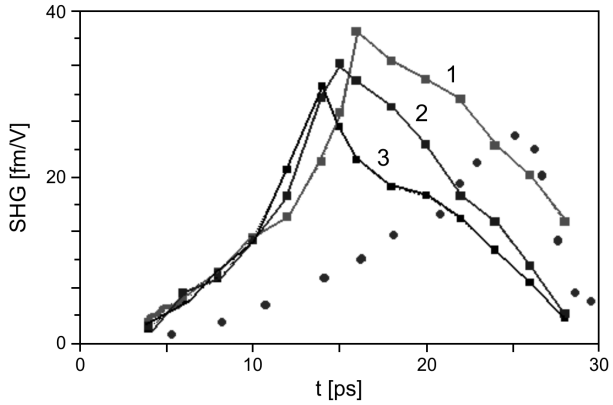

Fig. 3. Pump-probe delaying dependences of the LEOE (●) and the SHG (■) at different temperatures: 4.2 K (1), 12 K (2), 25 K (3).

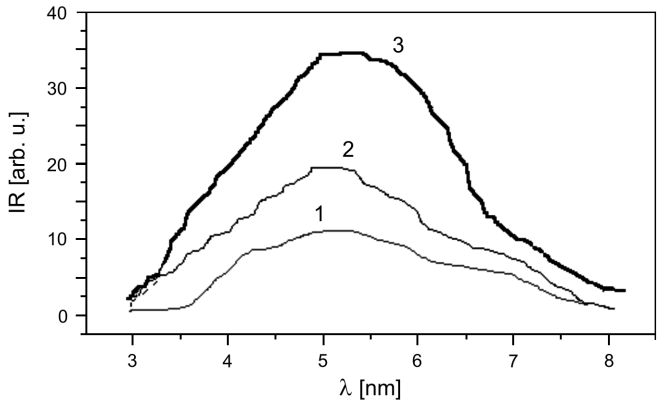

Fig. 4. Photoinduced spectral dependences of the IR modes *vs.* wavelength λ at different power densities: 0.5 GW/cm^2 (1), 1.0 GW/cm^2 (2), 1.5 GW/cm^2 (3) at 4.2 K.

ones due photoinduced anharmonic phonon modes $\Omega_1 \pm \Omega_2 \pm \Omega_3$. In this case, the occurrence of the non-polar components originating from the interactions between the doubled frequency and fundamental waves (see Fig. 3) was excluded.

In Figure 3 the typical dependences of the SHG and LEOE versus delaying pump-probe times are presented. Moreover for the SHG dependences the data for different temperatures were added. One of the differences of the IR poling compared to the electronic ones consisted in commensurable values of electronic and phonon dipole moments contributing to the appropriate nonlinear optical susceptibilities. It is the main reason why the delaying time between the LEOE and the SHG was different (see Fig. 3). The absence of the interactions with high power probing beams for the LEOE was one of the reasons of such shifting because the processes described by the Eqs. (4)–(6) were different.

To confirm the theoretical predictions about the dominant role of the EPI, the IR absorption spectra within the range of 4–7 μm were measured under the influence of CO-laser pumping beam at $T = 4.2$ K (see Fig. 4). An increase of CO-laser photoinducing beams favors the appearance of additional IR modes within the spectral range of 3–7 μm. Such an increase correlated well with the observed second-order optical effects and was a direct confirmation of the substantial contribution of the EPI to the output nonlinear optical susceptibilities obtained theoretically (see Fig. 1).

5. Summary

Principal occurrence of the observed effect was caused by great electron–phonon anharmonicity of the investigated glass. The macroscopic IR induced charge density non-centrosymmetry phenomenologically described by the fifth-order nonlinear optical susceptibility was predicted. The main difference in the present effect as compared with the traditional optical second harmonic generation consisted in substantial contributions of anharmonic electron–phonon subsystem induced by IR pumping laser. Using microscopic band energy approach, as well as the EPI photokinetics, the fifth-order nonlinear optical origin of the observed phenomenon was proved. Independent measurements of the photoinduced IR spectra directly indicated a good correlation between the number of the photoexcited IR modes and the observed SHG and LEOE. The time evolution of these effects is consistent with a simple model of electron–phonon anharmonic interactions. Moreover, the technique may be used quite widely in IR optical fibres, and may be applied to a wide variety of IR photoinducing processes, including two-photon absorption, nonlinear optical parametric oscillators and exciton-phonon interactions. The IR poling opens surely new perspectives in the tailoring of phase-matching glasses for frequency conversion.

Acknowledgements – The financial support from the Polish State Committee for Scientific Research (KBN), through the University (W. G.), is gratefully acknowledged.

References

[1] BOYD R., *Nonlinear Optics*, New York 1992.

[2] SHEN Y.R., *Introduction to Nonlinear Optics*, New York 1994.

[3] HOMOELLE D., WIELANDY S., GAETA A.L., BORRELLI N.F., SMITH C., *Infrared photosensitivity in silica glasses exposed to femtosecond laser pulses*, Optics Letters **24**(18), 1999, pp. 1311–13.

[4] GRUBSKY V., FEINBERG J., *Long-period fiber gratings with variable coupling for real-time sensing applications*, Optics Letters **25**(4), 2000, pp. 203–5.

[5] STEGALL D.B., ERDOGAN T., *Dispersion control with use of long-period fiber gratings*, Journal of the Optical Society of America A: Optics, Image Science and Vision **17**(2), 2000, pp. 304–12.

[6] DODGE J.S., SCHUMACHER A.B, BIGOT J.-Y., CHEMLA D.S., INGLE N., BEASLEY M.R., *Time-resolved optical observation of spin-wave dynamics*, Physical Review Letters **83**(22), 1999, pp. 4650–3.

[7] GAUTIER C.A., LEFUMEUX C., ALBERT O., ETCHEPARE J., *Spectral content of time resolved electronic and phonon induced non-linearities*, Optics Communications **178**(1-3), 2000, pp. 217–24.

[8] ANTONYUK B.P., *All optical poling of glasses*, Optics Communications **181**(1-3), 2000, pp. 191–5.

[9] PRIMOZICH N., SHAHBAZYAN T.V., PERAKIS I.E., CHEMLA D.S., *Coherent ultrafast optical dynamics of the Fermi-edge singularity*, Physical Review B: Condensed Matter **61**(3), 2000, pp. 2041–58.

[10] ZHAO X., XU L., YIN H., SAKKA S., *Glass formation in Sb_2Se_3–MX_n (metal halides)*, Journal of Non-Crystalline Solids **167**(1-2), 1994, pp. 70–3.

[11] KITYK I.V., KASPERCZYK J., PLUCINSKI K., *Two-photon absorption and photoinduced second -harmonic generation in Sb_2Te_3–$CaCl_2$–$PbCl_2$ glasses*, Journal of the Optical Society of America B: Optical Physics **16**(10), 1999, pp. 1719–24.

[12] KITYK I.V., SAHRAOUI B., *Photoinduced two-photon absorption and second-harmonic generation in As_2Te_3–$CaCl_2$–$PbCl_2$ glasses*, Physical Review B: Condensed Matter **60**(2), 1999, pp. 942–9.

[13] HISAKUNI H., TANAKA K., *Giant photoexpansion in As_2S_3 glass*, Applied Physics Letters **65**(23), 1994, pp. 2925–7.

[14] DALAL N., KLYMACHYOV A., BUSSMANN-HOLDER A., *Coexistence of order-disorder and displacive features at the phase transitions in hydrogen-bonded solids: squaric acid and its analogs*, Physical Review Letters **81**(26), 1998, pp. 5924–7.

[15] FIORINI C., CHARRA F., NUNZI J.-M., *Six-wave mixing probe of light-induced second-harmonic generation: example of dye solutions*, Journal of the Optical Society of America B: Optical Physics **11**(12), 1994, pp. 2347–58.

[16] DAVYDOV A.S., *Introduction to the Solid State Physics*, Nauka, Moscow, 1997 (in Russian).

[17] BACHELET G.B., HAMANN D.R., SCHLUTER M., *Pseudopotentials that work: from H to Pu*, Physical Review B: Condensed Matter **26**(8), 1982, pp. 4199–228.

[18] KITYK I.V., KASPERCZYK J., ANDRIEVSKII B.V., *Energy band structure of $KLiSO_4$ single crystals*, Physics Letters A **216**(1-5), 1996, pp. 161–6.

[19] KITYK I.V., *IR-stimulated second harmonic generation in Sb_2Te_2 Se–BaF_2–$PbCl_2$ glasses*, Journal of Modern Optics **51**(8), 2004, pp. 1179–89.

[20] ETILE A.-C., FIORINI C., CHARRA F., NUNZI J.-M., *Phase-coherent control of the molecular polar order in polymers using dual-frequency interferences between circularly polarized beams*, Physical Review A: Atomic, Molecular, and Optical Physics **56**(5), 1997, pp. 3888–96.

[21] MAKER P.D., TERHUNE R.W., NISENOFF M., SAVAGE C.M., *Effects of dispersion and focusing on the production of optical harmonics*, Physical Review Letters **8**, 1962, pp. 21–2.

[22] MELANCHOLIN A., *Principles of Measurements in the Crystallooptics*, Nauka, Moscow 1974 (in Russian).

Received June 6, 2005
in revised form November 5, 2005